

Symmetry Protected Quantum State Renormalization

Ching-Yu Huang,¹ Xie Chen,² and Feng-Li Lin³

¹*Max-Planck-Institut für Physik komplexer Systeme, 01187 Dresden, Germany**

²*Department of Physics, University of California at Berkeley, Berkeley, CA 94720, USA[†]*

³*Department of Physics, National Taiwan Normal University, Taipei, 116, Taiwan[‡]*

Symmetry protected topological (SPT) phases with gapless edge excitations have been shown to exist in principle in strongly interacting bosonic/fermionic systems and it is highly desirable to find practical systems to realize such phases through numerical calculation. A central question to be addressed is how to determine the SPT order in the system given the numerical simulation result while no local order parameter can be measured to distinguish the phases from a trivial one. In the tensor network approach to simulate strongly interacting systems, the quantum state renormalization algorithm has been demonstrated to be effective in identifying the intrinsic topological orders. Here we show that a modified algorithm can identify SPT orders by extracting the fixed point entanglement pattern in the ground state wave function which is essential for the existence of SPT order. The key to this approach is to add symmetry protection to the quantum state renormalization process and we demonstrate the effectiveness of this algorithm with the example of AKLT states in both 1D and 2D.

CONTENTS

| | |
|--|----|
| I. Introduction | 1 |
| II. Review | 2 |
| A. Symmetry protected topological order | 2 |
| B. Quantum state renormalization group | 3 |
| III. Symmetry protected quantum state renormalization | 6 |
| A. One-dimensional case | 6 |
| 1. Algorithm | 6 |
| 2. 1-dimensional AKLT state as the example | 8 |
| B. Two-dimensional case | 8 |
| 1. Algorithm | 9 |
| 2. 2-dimensional AKLT phase as the example | 9 |
| IV. Conclusion | 10 |
| Acknowledgments | 11 |
| A. Projective Representation | 11 |
| B. Numerical results for solving 2-dimensional AKLT-like model | 11 |
| References | 12 |

I. INTRODUCTION

Symmetry protected topological (SPT) phases are bulk-gapped quantum phases with symmetries [1]. If the system is on a closed manifold, the ground state does not spontaneously break the symmetry. On the other hand, if the system has a boundary, there are gapless or degenerate edge states as long as the symmetries are not explicitly broken. Therefore SPT phases represent a non-trivial type of order beyond Landau's symmetry breaking theory. Topological insulators and superconductors are examples of SPT phases in free fermion systems [2–7]. In one spatial dimension, a complete understanding of all possible SPT phases in interacting systems has been obtained [8–14] starting from the classic example of Haldane phase in spin 1 chains [15, 16]. Recently, it has been discovered that nontrivial SPT orders can also exist in strongly interacting boson/fermion systems in two and higher dimensions [1, 18]. Exactly solvable models were presented which has a gapped and symmetric bulk and gapless symmetry protected edge states [18–20].

It is highly desirable to find such strongly interacting SPT phases in experiments, similar to their free fermion counterparts. While the exactly solvable models prove the existence of SPT orders in strongly interacting systems, it is very unlikely that such models can be realized in experiments. In order to determine which physically realistic systems can have SPT order, numerical simulations are necessary. The tensor network renormalization algorithm [21–25] is a powerful and generic approach to simulate strongly interacting boson/fermion systems in two and higher dimensions and therefore can play a major role in the discovery of strongly interacting SPT orders.

A major question to be addressed in the tensor network approach to simulate SPT phases is how to identify the SPT order. Symmetry breaking phases can be identified by measuring local order parameters in the ground states. However, as SPT ground states do not break any

* aya.joa@pks.mpg.de

† xiechen@berkeley.edu

‡ linfengli@phy.ntnu.edu.tw

symmetry, no local measurement can distinguish an SPT phase from a trivial symmetric phase. Systems with intrinsic topological order (like Z_2 spin liquids or fractional quantum Hall systems) on the other hand can be identified by measuring the ground state degeneracy on a torus [26, 27] or the topological entanglement entropy [28, 29]. However, these quantities are both trivial for SPT states.

An important signature of SPT phases is the existence of nontrivial entanglement structure in their ground states [1, 19]. Compared to trivial symmetric phases whose ground states can be simple product states (for example the $\prod(|\uparrow\rangle + |\downarrow\rangle)$ state in the transverse field Ising model), the entanglement structure in the ground states of SPT phases cannot be totally removed as long as symmetry is not broken. Therefore, SPT ground states are characterized by short-range entanglement which is protected by symmetry. This is similar to systems with intrinsic topological orders where the long-range entanglement patterns in the ground states are essential for the existence of the order. It has been shown that the long-range entanglement patterns can be effectively extracted using a quantum state renormalization algorithm based on the tensor network representation of the ground states [30, 31]. Can similar ideas be applied to SPT orders?

Naively, one might expect that the quantum state renormalization algorithm fails to distinguish SPT order from trivial symmetric phases, as the algorithm is designed to remove short range entanglement structures from the state and retain only the long-range one. After removing all short range entanglement, the ground state of SPT phases becomes a total product state which is the same as a trivial symmetry state. However, this is only possible if the symmetry of the system is broken during the process. If we require that symmetry is always preserved during the renormalization procedure, some short-range entanglement structures are always kept which can be used to identify the SPT order at the renormalization fixed point.

In this paper, we show how such a symmetry protection can be properly added to the quantum state renormalization algorithm. In particular, we demonstrate the effectiveness of our algorithm by applying it to the 1D and 2D AKLT phases and show that the SPT order in these systems can be successfully identified from the fixed point short-range entanglement pattern of the states. The paper is organized as follows: in section II, we review the notion of SPT order (especially that in AKLT state) and the quantum state renormalization algorithm which can be used to identify intrinsic topological orders; section III discusses how symmetry protection can be added to the quantum state renormalization procedure and how it can be used to identify the SPT order in 1D and 2D AKLT states which allows us to determine the phase diagram of 1D and 2D anti-ferromagnetic spin models; in section IV we conclude our discussion and talk about open questions. In Appendix A we briefly review the notion of projective representation; some numerical results of solving 2D AKLT-like model are given in Appendix B.

II. REVIEW

A. Symmetry protected topological order

Symmetry protected topological (SPT) order is characterized by the robust gapless edge modes of a bulk gapped phase without intrinsic topological order or spontaneously symmetry breaking. These gapless edge modes are protected as long as the protecting symmetry of the system is unbroken. A simple example of an SPT phase is the topological insulator in free fermion systems [2–4]. For systems with interaction, the SPT phases can be classified by group cohomology [1]. The key observation used in this classification method is that the edge of a d -dimensional SPT phase forms a local $d - 1$ dimensional system with a special symmetry action. For example, in 1-dimensional (1D) SPT phases, the edge states are point (0-dimensional) degrees of freedom forming the projective representations of the symmetry group while the physical degrees of freedom in the system all form linear representations. Projective representations of a symmetry group are classified by the second group cohomology $H^2(G, U(1))$. See Appendix A for a brief introduction of projective representation. In higher dimensions, symmetry on the edge of an SPT phase can act in a non-onsite way related to the higher cohomology groups of the symmetry group. Moreover, if translation symmetry is present besides on-site symmetry, higher dimensional SPT phases can be obtained by stacking lower dimensional ones. In this paper, we are focusing on the 1D SPT phase with on-site $SO(3)$ rotation symmetry and the two dimensional SPT phase with both on-site $SO(3)$ symmetry and translation symmetry which can be obtained by stacking the 1D phases along different directions. In the following we are going to review our understanding of these phases using the example of AKLT states.

One dimensional spin 1 Haldane chain with antiferromagnetic interaction

$$H_{Haldane} = \sum_i \vec{S}_i \vec{S}_{i+1} \quad (1)$$

was the first known example of an SPT phase [15]. It was realized that the bulk of the system is gapped. However if the system is put on an open chain, the ground state will be four-fold degenerate with two fold degeneracy coming from each end of the chain. This result is most easily understood at an exactly solvable point in the same phase called the AKLT point with Hamiltonian [16]

$$H_{1D \text{ AKLT}} = \sum_i \vec{S}_i \vec{S}_{i+1} + \frac{1}{3} (\vec{S}_i \vec{S}_{i+1})^2 \quad (2)$$

The ground state wavefunction was shown to be of a valence bond structure as shown in Fig.1 where each spin 1 decomposes into two spin 1/2's and the spin 1/2's form singlets $|\uparrow\rangle|\downarrow\rangle - |\downarrow\rangle|\uparrow\rangle$ between nearest neighbor sites. The total wave function is a product of such singlets between

site i and $i+1$. It is then clear that the bulk of the system does not break symmetry and is short range entangled. Any excitation in the bulk can be gapped. However, if the system is open, there will be dangling spin $1/2$'s left at the end of the chain, giving rise to two fold degeneracy as long as $SO(3)$ rotation symmetry is not broken. Therefore, the AKLT state, as well as the whole Haldane phase, has $SO(3)$ symmetry protected topological order. It has been shown that the 1D Haldane phase is continuously connected without breaking symmetry to the dimer state where each site contains the full Hilbert space of two spin $1/2$'s and the spin $1/2$'s form singlets between nearest neighbor sites[32, 33]. That is, we can adiabatically turn off the projection of two spin $1/2$'s per site to a total spin 1 without affecting the SPT order in the phase. The dimer state is a tensor product of local entangled singlet pairs and has 0 correlation length. Therefore, it is a fixed point representative of the Haldane phase.



FIG. 1. Valence bond structure of AKLT ground state in 1D. Each big oval represents a spin 1 and each small circle represents a spin $1/2$. Connected circles are spin $1/2$ singlets.

The degeneracy of edge spin $1/2$ is not only stable against any perturbation of the spin 1 chain which is $SO(3)$ symmetric, it is also stable even if addition or removal of local degrees of freedom are allowed as long as they form linear representations of $SO(3)$, i.e. they are integer spins. It is necessary to consider the second stability condition because, when a system is perturbed, it is possible that more degrees of freedoms (e.g. orbitals, bands) get involved in the interaction. The symmetry requirement on the system cannot exclude the possibility that symmetric local degrees of freedom (linear representations of symmetry groups) to be added or removed. The spin 1 Haldane chain is stable even this is allowed as the fractional edge spin $1/2$ cannot become a trivial spin 0 through interaction with any integer spin. However, the spin 1 edge state in the spin 2 AKLT state with similar valence bond structure can be removed by adding an extra spin 1 to the edge which forms a singlet with the original edge spin 1. Therefore, the spin 2 AKLT state is in a trivial SPT phase. Its edge state degeneracy is not protected under $SO(3)$ rotation symmetry. The difference between trivial and nontrivial 1D SPT phases can be most clearly seen from the edge where the former hosts an integer spin and the latter hosts a half integer spin. Such a distinction can be generalized to any symmetry group where edge states forming projective representations correspond to nontrivial SPT phases while edge states forming linear representations correspond to trivial ones. (See Appendix A for definition of projective representation.) The distinction between integer/half integer spins (linear and projective representations) is the key to our understanding of $SO(3)$ symmetric SPT phases and

will play an important role in our discussion of quantum state renormalization group transforms below.

The valence bond picture of the 1D AKLT state can be generalized to 2D [17], giving rise to a 2D SPT phase protected by both $SO(3)$ and translation symmetry. Consider the 2D state on a honeycomb lattice with one spin $3/2$ per site. The spin $3/2$ can be decomposed into three spin $1/2$'s each forming a spin singlet with another spin $1/2$ on a neighboring site, as shown in Fig. 2.

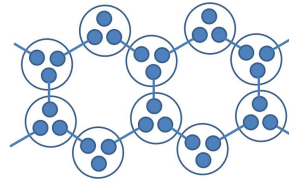


FIG. 2. Valence bond structure of AKLT ground state on 2D honeycomb lattice. Each big circle represents a spin $3/2$ and each small circle represents a spin $1/2$. Connected circles are spin $1/2$ singlets.

The bulk of the system is again symmetric and gapped. On the edge of the system, there is a chain of spin $1/2$ left uncoupled. Perturbations to the edge may couple these spin $1/2$'s. However, as long as the perturbation preserves $SO(3)$ and certain translation symmetry of the honeycomb lattice, the edge state is gapless [40]. Therefore, the 2D AKLT state is in a 2D SPT phase protected by $SO(3)$ and translation symmetry. The fixed point representative of this phase is again the dimer state which is a product of singlet pairs between nearest neighbor sites.

B. Quantum state renormalization group

The renormalization group (RG) transformation is a mathematical tool to average over the short distance degrees of freedom, and can be used to demonstrate the universality of the phases at the RG fixed-point. Extending Wilson's original idea of RG, an efficient algorithm was proposed, called the density matrix renormalization group (DMRG) algorithm [34] to solve for the ground state of 1D noncritical systems by removing the short range entanglement before coarse graining. The DMRG algorithm can be conceptually thought of a variational algorithm based on matrix product states ansatz. For 1D critical systems and also systems of higher dimension, algorithms based on tensor product states and the Multi-scale Entanglement Renormalization Ansatz were also proposed to simulate ground state, based on related RG ideas of removing local entanglement and coarse graining[21–23].

Here, we will consider the Quantum State Renormalization Group (QSRG) transformation which, instead of simulating the quantum state of a system, aims to extract the universal properties of a system from the description of its ground state wave function. The basic

idea is to remove nonuniversal short range entanglement structures related to the microscopic details of the system from the wave function before coarse graining. After many rounds of QSRG the original ground state can flow to a simpler fixed-point state. We may then identify or even classify the phases using the fixed-point states. Such a QSRG algorithm was first shown to be executable based on the matrix product state description of 1D quantum states[35] which was used for the classification of 1D gapped phases. The algorithm was further generalized to 2D tensor product states, which was demonstrated to be effective in identifying symmetry breaking phases and phases with intrinsic topological order[30]. Our discussion in this paper is based on these two algorithms and we review them below.

The original procedure of the 1D QSRG is as follows [35]. The algorithm is based on the matrix product state (MPS) description of a 1D quantum state given by

$$|\phi\rangle = \sum_{i_1, i_2, \dots, i_N} \text{Tr}(A^{i_1} A^{i_2} \dots A^{i_N}) |i_1 i_2 \dots i_N\rangle \quad (3)$$

where $i_k = 1 \dots d$ with d being the physical dimension of a spin at each site, A^{i_k} 's are $\chi \times \chi$ matrices related to the physical state $|i_k\rangle$ with χ being the inner dimension of the MPS.

In the first step of the QSRG procedure, one merges two neighboring sites, says the sites $2i - 1$ and $2i$ into a new site. In terms of the matrices A^s , that means forming a new matrix \tilde{A} as

$$\tilde{A}_{\alpha\beta}^{(pq)} \equiv \sum_{\gamma=1}^{\chi} A_{\alpha\gamma}^p A_{\gamma\beta}^q. \quad (4)$$

One further performs the singular value decomposition

$$\tilde{A}_{\alpha\beta}^{(pq)} \equiv \sum_{l=1}^{\min(d^2, \chi^2)} U_l^{\dagger(pq)} \lambda V_{(\alpha\beta)}^l, \quad (5)$$

where (pq) means the combined physical indices.

Here, one keeps only the relevant degrees of freedom indicated by the upper bound $\min(d^2, \chi^2)$ of the above sum. These two steps correspond to one round of RG transformation. After performing n such steps, The Hilbert space of each local site is d^{2^n} -dimensional and corresponds to 2^n original sites. However, for the noncritical spin chains, the block entanglement entropy will be saturated to a finite value. This implies that only few degrees of freedom couple to the outer sites. From quantum information perspective, there will exist a unitary transformation that could transform the d^{2^n} -dimensional space into a smaller one. The relevance of the degrees of freedom is indicated by the magnitude of the eigenvalues of the block reduced density matrix. In the MPS representation, the dimension of Hilbert space of the block remains bounded above by χ^2 as can be seen from the singular value decomposition. In this way, it is possible to perform the

coarse-graining without any truncation for gapped MPS with a finite χ .

The matrix U in (4) is the aforementioned unitary transformation which connects the old and new MPS's after one round of QSRG, that is

$$A^p \xrightarrow{RG} A'^l = \lambda^l V^l. \quad (6)$$

In summary, after one round of QSRG transformation of merging two neighboring sites, the state $|\psi\rangle$ is transformed as follows:

$$|\psi\rangle \rightarrow |\tilde{\psi}\rangle = U_{1,2} \otimes U_{3,4} \otimes \dots \otimes U_{2i-1,2i} \otimes \dots |\psi\rangle. \quad (7)$$

Then we can combined the new sites and perform another round of RG. The procedure is illustrated in Fig.3

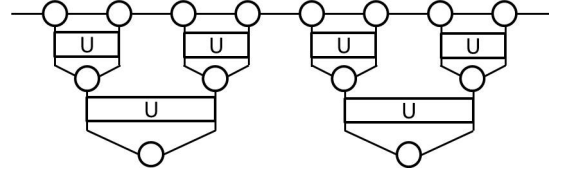


FIG. 3. Quantum state renormalization group procedure as given in [35].

For comparison with the 2D version of the QSRG procedure, we need to rephrase the steps of the 1D QSRG procedure using the notion of the double tensor of a MPS. The double tensor of an MPS with matrices A^i 's is given by

$$\mathbb{E}_{\alpha\gamma, \beta\chi} = \sum_i A_{\alpha\beta}^i \times (A_{\gamma\chi}^i)^* \quad (8)$$

An important property of \mathbb{E} is that it uniquely determines the matrices, and hence the state, up to a local change of basis on each site [41, 42]. That is, if

$$\mathbb{E}_{\alpha\gamma, \beta\chi} = \sum_i A_{\alpha\beta}^i \times (A_{\gamma\chi}^i)^* = \sum_i B_{\alpha\beta}^i \times (B_{\gamma\chi}^i)^* \quad (9)$$

then $A_{\alpha\beta}^i$ and $B_{\alpha\beta}^i$ are related by a unitary transformation U :

$$B_{\alpha\beta}^i = \sum_j U_{ij} A_{\alpha\beta}^j. \quad (10)$$

Renormalization transformations on the MPS, including the local unitary operations and the coarse graining, can be applied through manipulations of \mathbb{E} . Treat \mathbb{E} as a $\chi^2 \times \chi^2$ matrix with row index $\alpha\gamma$ and column index $\beta\chi$. Combine the double tensor of the two sites together into $\tilde{\mathbb{E}} = \mathbb{E}\mathbb{E}$. Then think of $\tilde{\mathbb{E}}_{\alpha\gamma, \beta\chi}$ as a matrix with row index $\alpha\beta$ and column index $\gamma\chi$. It is easy to see that with such a recombination, \mathbb{E} is a positive matrix and can be diagonalized

$$\tilde{\mathbb{E}}_{\alpha\gamma, \beta\chi} = \sum_{\tilde{i}} \lambda_{\tilde{i}} V_{\tilde{i}, \alpha\beta} V_{\tilde{i}, \gamma\chi}^*, \quad (11)$$

where we have kept only the non-zero eigenvalues $\lambda_{\tilde{i}}$ and the corresponding eigenvectors $V_{i,\alpha\beta}$. \tilde{A} is then given by

$$\tilde{A}_{\alpha\beta}^{\tilde{i}} = \sqrt{\lambda_{\tilde{i}}} V_{i,\alpha\beta}, \quad (12)$$

which are the matrices representing the new state. Here \tilde{i} correspond to the combined index of pq above. Using double tensor \mathbb{E} , we have implemented the same RG procedure for 1D MPS as given by (4) and (5).

For 1D MPS, one can do the exact coarse graining without any truncation to the inner dimensions of the matrices due to the finite amount of entanglement between any segment of the chain and the rest of the system. However, in two dimension we need to find a local unitary transformation which removes the short range entanglement and discards the irrelevant degrees of freedoms before coarse graining. Such a procedure for 2-dimensional tensor product state (TPS) has been given in [30]. It was shown that the algorithm can remove short range entanglement in a 2-dimensional TPS and identify the long range entanglement structure, hence the topological order, from the fixed point tensors. Here we review the basic procedure given in [30].

A TPS is characterized by an on-site tensor $T_{\alpha\beta\gamma\dots}^i$ with physical index i and internal indices $\alpha\beta\gamma$ etc. The wave function is given in terms of these tensors by

$$|\psi\rangle = \sum_{i_1, i_2, \dots, i_m \dots} \text{tTr}(T^{i_1} T^{i_2} \dots T^{i_m} \dots) |i_1 i_2 \dots i_m \dots\rangle \quad (13)$$

where tTr denotes tensor contraction of all the connected inner indices according to the underlying lattice structure. Without loss of generality, we consider the honeycomb lattice here. The procedure of QSRG is to flow the tensor T to its fixed-point form. To do this, we first form a positive double tensor \mathbb{T}_1 by merging two layers of tensors T and its hermitian conjugate T^\dagger with the physical indices contracted as shown in Fig. 4, namely,

$$\mathbb{T}_{1;\alpha'\gamma'\epsilon',\alpha\gamma\epsilon} = \sum_i (T_{\alpha'\gamma'\epsilon'}^i)^* \times T_{\alpha\gamma\epsilon}^i \quad (14)$$

Note that the resultant double tensor is invariant under local unitary transformations by construction. Similarly, we can form another double tensor \mathbb{T}_2 on the neighboring site of \mathbb{T}_1 . Merging \mathbb{T}_1 and \mathbb{T}_2 to form a new double tensor \mathbb{T} with 4 legs, i.e.,

$$\mathbb{T}_{\alpha'\beta'\gamma'\delta',\alpha\beta\gamma\delta} = \sum_{\epsilon,\epsilon'} \mathbb{T}_{1;\alpha'\gamma'\epsilon',\alpha\gamma\epsilon} \mathbb{T}_{2;\epsilon'\beta'\delta',\epsilon\beta\delta}. \quad (15)$$

This completes the step (1) of Fig. 4.

We then spectrally decompose the double tensor, i.e., \mathbb{T} , i.e.,

$$\mathbb{T}_{\alpha'\beta'\gamma'\delta',\alpha\beta\gamma\delta} = \sum_j \lambda_j (\hat{T}_{\alpha'\beta'\gamma'\delta'}^j)^* \times \hat{T}_{\alpha\beta\gamma\delta}^j. \quad (16)$$

With the above spectral decomposition, we form a new tensor \tilde{T} with the physical indices labeled by l, m, n, r , as

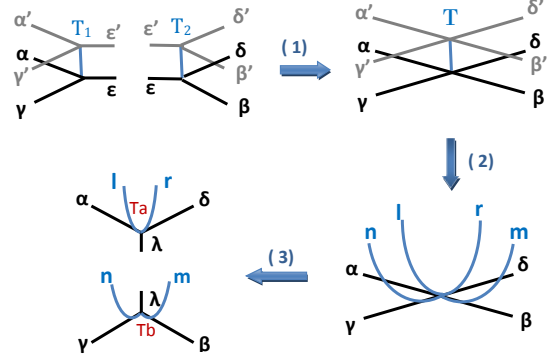


FIG. 4. The QSRG procedure on honeycomb lattice (part 1): In the step (1), combining double tensor \mathbb{T}_1 and \mathbb{T}_2 on the neighboring sites into a double tensor \mathbb{T} . In the step (2), decomposing the double tensor \mathbb{T} into the tensor \tilde{T} . In the step (3), decomposing the tensor \tilde{T} , resulting in tensors T_a , T_b .

shown in the step (2) of Fig. 4, i.e.,

$$\tilde{T}_{\alpha\beta\gamma\delta}^{lmnr} = \sum_j \sqrt{\lambda_j} (\hat{T}_{lmnr}^j)^* \times \hat{T}_{\alpha\beta\gamma\delta}^j. \quad (17)$$

The spectral weights encode the relevance of the entangled components. In this step one has removed the SRE by the local unitary transformation which takes the tensor T into \tilde{T} according to the significance of the spectral weights. This is similar to the disentangler in the multi-scale entanglement renormalization ansatz (MERA) [37] before the coarse-graining. Then, we do a singular value decomposition of \tilde{T} in the direction orthogonal to the link between \mathbb{T}_1 and \mathbb{T}_2 , and decompose tensor \tilde{T} into T_a and T_b as shown in the step (3) of Fig. 4, i.e.,

$$\tilde{T}_{\alpha\beta\gamma\delta}^{lmnr} = \sum_{\lambda} T_{a;\alpha,\delta\lambda}^{ln} \times T_{b;\beta\epsilon\lambda}^{mr}. \quad (18)$$

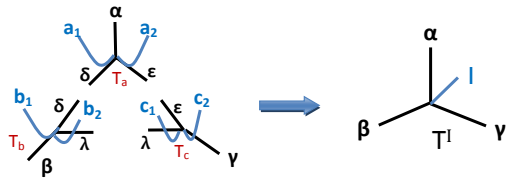


FIG. 5. The QSRG procedure on honeycomb lattice (part 2): Merge three tensors T_a , T_b and T_c around a triangle to form a new tensor T^I .

Next, we coarse grain the lattice labelled by the tensor \tilde{T} by implementing one step of block decimation in the TRG method [24]. To do this, we combine the resultant

three tensors that meet at a triangle to form a new tensor with physical index I as shown in the Fig. 5,

$$T_{\alpha\beta\gamma}^I = \sum_{\delta\epsilon\lambda} T_{a,\alpha\delta\epsilon}^{a_1a_2} \times T_{b,\beta\delta\lambda}^{b_1b_2} \times T_{c,\gamma\lambda\epsilon}^{c_1c_2}. \quad (19)$$

where I denotes the combination of all physical indices a_1, a_2, b_1, b_2, c_1 and c_2 . This new tensor is the resultant one after one round of QSRG proposed in [30].

After repeating the above QSRG procedure, the original TPS will then flow into a fixed-point state with SRE removed but not the LRE. Therefore, we can use this method to find out the possible topologically ordered phases by examining the fixed-point tensor. Moreover, this method is easy to be implemented numerically and has been used to identify and study phases with intrinsic topological order, for example see [31].

III. SYMMETRY PROTECTED QUANTUM STATE RENORMALIZATION

Though the above QSRG procedure is quite powerful in identifying the intrinsic topological orders, it is not suitable when we consider SPT orders. This is because, the above QSRG procedure is designed to remove short range entanglement, which makes SPT orders indistinguishable from trivial orders. Indeed, consider applying the above QSRG procedure to the 2D dimer state on the honeycomb lattice. Each bond originally has a dimer state on it. When applying the steps in Fig.4, the dimer on the horizontal bond shrinks and no dimer state is regenerated when splitting in the vertical direction. After several rounds of RG, it is easy to see that the dimer structure can be completely removed, resulting in a total product state with no SPT order.

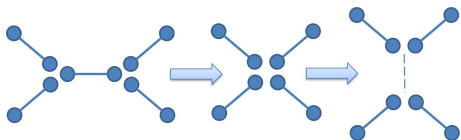


FIG. 6. Applying QSRG procedure given in [30] to 2D dimer state. After applying steps in Fig.4, the dimer on the middle bond gets removed. The dimer structure can be completely removed after a couple rounds of RG.

The key reason that the dimer state flows to a trivial state under the QSRG scheme is because the symmetry of the system is not preserved when doing local unitary transformations or coarse graining transformations on the state. Therefore, we need to find a way to explicitly incorporate the symmetry of the system into the RG scheme in order to preserve the short range entanglement structure of SPT states in the RG flow. In this section, we will propose such a symmetry protected QSRG procedure for TPS and demonstrate its effectiveness in identifying the SPT order from fixed point tensors.

In order to devise the 2D procedure, let's start with the simpler 1D case. The 1D QSRG procedure as given in [35] does preserve the short range entanglement structure in the fixed point tensor of 1D AKLT state, hence allowing the identification of the SPT order. However, a major difference between 1D and 2D QSRG is that, in 1D the amount of entanglement of a segment of an MPS is bounded, therefore we can perform coarse graining without explicitly removing short range entanglement. In 2D, this is not the case. The amount of entanglement of a region in a TPS grows linearly with the length of its boundary, therefore straightforward coarse graining would lead to unbounded growth of entanglement and hence unbounded growth in the size of the representing tensor. In order to maintain a bounded numerical complexity during the RG procedure, it is important that irrelevant entanglement structures are removed using, for example, the merging and splitting procedure as shown in Fig. 4. The key to our symmetry protected RG scheme is then to preserve symmetry in the merging and splitting procedure. Before we do this in 2D, let's first add the merging and splitting procedure into 1D RG scheme and show how symmetry protection can be incorporated.

A. One-dimensional case

1. Algorithm

To construct such a symmetry protected QSRG, the key problem is how to preserve the symmetric SRE in the process of QSRG. We will adopt the main procedure of the 1D QSRG as schematically given in Fig. 8 but with some essential modifications to preserve the symmetric SRE.

Assume the ground state considered is represented in the MPS denoted by a three-rank tensor $T_{\alpha,\beta}^i$, where i is the physical index and α, β are the left and right indices of the inner bond, respectively. In the following we will assume translational invariance so that the tensor T is the same for all sites. Our proposed symmetry protected QSRG is implemented as follows. Firstly, we form a positive double tensor by merging two layers of tensors with physical indices contracted (as shown in the Fig. 7 after step 1).

$$\mathbb{T}^i = \sum_j (T_{\alpha',\gamma'}^i)^* \times T_{\alpha,\gamma}^i. \quad (20)$$

We then merge two neighboring sites, says the sites $i-1$ and i , into a new block tensor \mathbb{T}' (as shown in the Fig. 7 after step 3). Perform the spectral decomposition as before, i.e.,

$$\mathbb{T}'_{\alpha,\gamma,\alpha',\gamma'} = \sum_j \lambda_j (\hat{T}_{\alpha',\beta'}^j)^* \times \hat{T}_{\alpha,\beta}^j. \quad (21)$$

With such a spectral decomposition we can form a new

tensor \tilde{T} as follow:

$$\tilde{T}_{\alpha,\gamma}^{a,b} = \sum_i \sqrt{\lambda_i} \hat{T}_{a,b}^i \times \hat{T}_{\alpha,\beta}^i. \quad (22)$$

As mentioned, this step is to perform a local unitary transformation on two neighboring sites to remove the SRE as the disentangler in MERA.

Next we need to coarse grain the lattice by first splitting the tensor \tilde{T}^I into two tensors T'^{s_1} and T'^{s_2} by performing singular value decomposition. We then merge two neighboring T' tensors, say the i -th and the $(i+1)$ -th ones to form a new site tensor T'' , i.e.,

$$T_{\alpha,\gamma}^{''I} = \sum_{\epsilon} T_{\alpha,\epsilon}^{''i,s_1} \times T_{\epsilon,\gamma}^{''i,s_2}. \quad (23)$$

This will complete one round of QSRG as for the 2-dimensional case. Schematically the whole procedure on the tensors is shown in Fig. 7 and the corresponding renormalization operation on the quantum state is shown in Fig. 8. However, the key point is whether we can preserve the SPT phase during the above process.

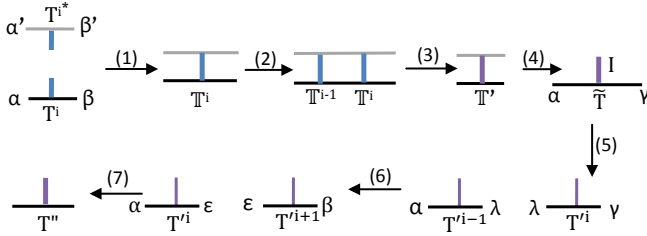


FIG. 7. Schematic procedure of the symmetry protected QSRG.

To preserve the SPT phase, we should assure that the symmetry property for the SPT phase is not destroyed during QSRG. Roughly, the above procedure is divided into disentangling and coarse-graining. For disentangling, the on-site symmetry is preserved by the local unitary transformation as it acts on the double tensor for which the physical indices are contracted.

As for the coarse-graining, it is possible to destroy the SPT when splitting and re-merging the neighboring site tensors. The symmetry properties of the site tensors for a SPT phase will manifest in the degeneracy patterns of the singular values when decomposing \tilde{T} into T' 's as shown in (22) and (23). If there are such degeneracy patterns, it means that the SRE encoded in these singular values is symmetry protected. We then should be careful in assigning appropriate representation for the physical legs according to the degeneracy patterns of the singular values before re-merging two neighboring sites. To do this, we should apply some symmetry generators to the MPS to “measure” the quantum number of the site tensor and then decide the appropriate representation.

According to the classification of the SPT phases by the using the group cohomology [1], we should make sure

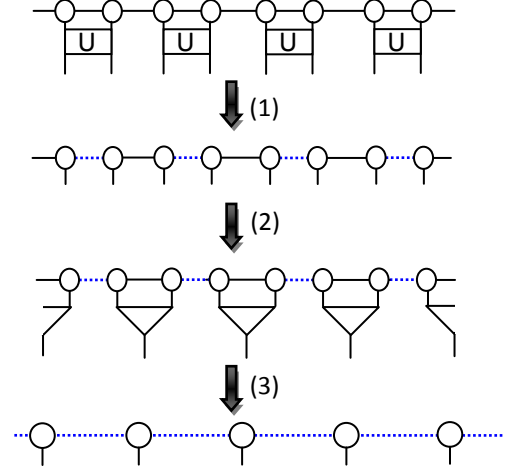


FIG. 8. Schematic procedure of the revised 1D QSRG given by (20)-(22). The step (1) is to remove the SRE by performing local unitary transformations. The steps (2) and (3) are to coarse grain the lattice by removing the local degrees of freedoms and merging two sites.

that all the site tensors in each step is in the same cohomology class. In practice, this will mean that the physical leg of the site tensor should remain in the same cohomology class to preserve the SPT order. Therefore, when we split the site tensor \tilde{T} , we should make sure the physical leg of the resultant tensor T' is in the same class of the group representations as the one for \tilde{T} . If necessary, we should enlarge the Hilbert space of the physical leg of \tilde{T} when splitting. Moreover, we should assign the appropriate representation for the physical leg by its measured quantum numbers so that the tensor T' is in the same cohomology class.

For example, if the on-site symmetry in protecting the SPT is $SO(3)$, then the representations for the integer spins and the half-integer spins are in different group cohomology classes. Therefore, when we split the spin 1 physical leg of the site tensor \tilde{T} , it may end up with two new site tensors whose physical legs can be interpreted either as in the spin 1/2 or spin 1 representations. We should manipulate the measured J and J_z quantum number and the possibility of enlarging the Hilbert space to make sure that the new site tensors have spin-1 physical leg.

To be more specific about the enlargement of the physical Hilbert space, here is the way of doing it: appending a singlet state, $\frac{1}{\chi} \sum_{k_1, k_2=1}^{\chi} C_{k_1, k_2} |k_1, k_2\rangle$, where C_{k_1, k_2} is a singlet state coefficient, as schematically shown in Fig. 9. Let us denote the state vector for the site tensor \tilde{T} to be

$$|\Psi\rangle = \sum_{a,b,\alpha,\gamma} \tilde{T}_{a,b,\alpha,\gamma} |\alpha\rangle |a\rangle |b\rangle |\gamma\rangle, \quad (24)$$

where a, b together are the physical indices, and α, γ are

the inner indices. Then, append a singlet state to enlarge the Hilbert space of the physical leg, i.e.,

$$|\Psi'\rangle = \sum_{a,b,\alpha,\gamma} \tilde{T}_{a,b,\alpha,\gamma} |\alpha\rangle|a\rangle|b\rangle|\gamma\rangle \otimes \frac{1}{\chi} \sum_{k_1,k_2=1}^{\chi} C_{k_1,k_2} |k_1, k_2\rangle \quad (25)$$

$$= \sum_{a,b,\alpha,\gamma,k_1,k_2} \Theta_{a,k_1,\alpha,b,k_2,\gamma} |\alpha\rangle|a\rangle|k_1\rangle|k_2\rangle|b\rangle|\gamma\rangle.$$

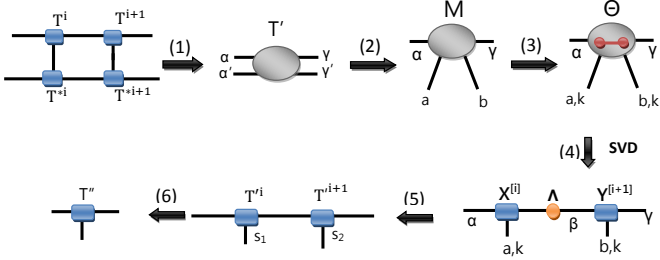


FIG. 9. A specific way of coarse-graining the MPS in the symmetry protected QSRG.

We can split the new site tensor Θ by performing the singular value decomposition so that

$$\Theta_{a,k,\alpha,b,k,\gamma} = \sum_{\beta} X_{(a,k,\alpha),\beta} \Lambda_{\beta} Y_{(b,k,\gamma),\beta} \quad (26)$$

Then, the new tensors T'^{s_1} and T'^{s_2} can be obtained from the tensor X and Y by attaching the Λ , i.e.,

$$T'^{s_1}_{\alpha,\beta} = \sqrt{\Lambda} \times X_{(a,k,\alpha),\beta}, \quad T'^{s_2}_{\beta,\gamma} = \sqrt{\Lambda} \times Y_{(b,k,\gamma),\beta}. \quad (27)$$

Finally, we merge two neighboring T' tensors to form a new one T'' as done in (23).

2. 1-dimensional AKLT state as the example

We now demonstrate how to apply the symmetry protected QSRG procedure discussed above to a concrete example of the SPT phase. Let us consider the 1-dimensional AKLT [16] MPS with $T^i = \sigma^i$, where σ^i ($i = x, y, z$) are the Pauli matrices. This AKLT state is shown to have SPT [8, 9, 43]. Moreover, as shown in [35], the fixed-point state of the original QSRG is the dimer state characterized by the transfer matrix $\sum_{i,j=1}^2 \frac{1}{4} |ii\rangle\langle jj|$ obtained from its MPS. As we mentioned, this QSRG does not destroy the symmetry and so preserves the SPT. Thus, we expect the dimer and AKLT states have the same SPT.

We now apply our symmetry protected QSRG to the AKLT MPS. We first perform the disentangler, and then the coarse-graining. When coarse-graining, we find that the singular value spectrum of the tensor \tilde{T} has one- and

three-fold degeneracies. This reflects the AKLT MPS has on-site $SO(3)$ symmetry protecting its SPT. This degeneracy pattern could be interpreted as combining two spin 1/2 sites, i.e., $2 \otimes 2 = 1 \oplus 3$. If we take this interpretation and perform the further splitting to obtain two T' tensors. Then, the physical leg of T' will be in spin 1/2 representation. We will obtain the fixed point double tensor, $\mathbb{T}_{1,1}^{1,1} = 1$, which is a product state. This is in the wrong cohomology class from the one of AKLT, whose physical leg should be in the integer spin representation.

To remedy this, we should measure the J and J_z quantum number of the singular value vectors, and then interpret the degeneracy pattern arising from combining two spin 1 sites, i.e., $3 \otimes 3 = 1 \oplus 3 \oplus 5$. We can then enlarge the Hilbert space of the physical leg by assigning the emptiness to the above 5-representation (spin 2) in the enlarged MPS, and identifying the 1-representation (spin 0) as $1/\sqrt{3}(|1, -1\rangle - |0, 0\rangle + |-1, 1\rangle)$, and the 3-representation (spin 1) as $1/\sqrt{2}(|1, 0\rangle - |0, 1\rangle)$, $1/\sqrt{2}(|1, -1\rangle - |-1, 1\rangle)$, and $1/\sqrt{2}(|0, -1\rangle - |-1, 0\rangle)$. Here $|s_1, s_2\rangle$'s with $s_{1,2} = -1, 0, 1$ are the basis vectors of $3 \otimes 3$. We then identify the labels $s_{1,2}$ as the ones for the physical legs of the two site tensors T' , respectively. In this way, we can split the tensor \tilde{T} to T' 's without destroying the SPT and then form the new tensor T'' to complete one step of our symmetry protected QSRG.

By this way, we can obtain the fixed point double tensor $\mathbb{T}_{\alpha,\beta}^{i,j}$ of AKLT state as follows:

$$\begin{aligned} \mathbb{T}_{11}^{11} &= 0.524, & \mathbb{T}_{22}^{11} &= 0.053, \\ \mathbb{T}_{12}^{12} &= 0.471, & \mathbb{T}_{21}^{21} &= 0.471, \\ \mathbb{T}_{11}^{22} &= 0.053, & \mathbb{T}_{22}^{22} &= 0.524. \end{aligned} \quad (28)$$

This is the same as the one for the dimer state obtained by the same symmetry protected QSRG procedure. It then justifies our symmetry protected QSRG in identifying the SPT.

We can also perform the coarse-graining of the symmetry protected QSRG in the way of Fig. 9 by appending a singlet state. In this way, we will obtain the following fixed-point double tensor for the AKLT state:

$$\begin{aligned} \mathbb{T}_{11}^{11} &= 0.5, & \mathbb{T}_{22}^{11} &= 0.5, \\ \mathbb{T}_{11}^{22} &= 0.5, & \mathbb{T}_{22}^{22} &= 0.5. \end{aligned} \quad (29)$$

Again, this is the same as the one for the dimer state obtained by the same symmetry protected QSRG procedure.

Note that the resultant double tensors in (28) and (29) are different. This reflects the fact that different SREs are removed during the process of QSRG. However, once we fix the way of QSRG, then both the AKLT and dimer states will flow to the same fixed-point double tensor.

B. Two-dimensional case

We will now generalize our symmetry protected QSRG to the 2D case. We first describe the algorithm for our

symmetry protected QSRG on the honeycomb lattice. Then, we study a deformed 2D AKLT model on honeycomb lattice, and show that there exist a possible SPT phase by calculating some order parameters. Finally, we demonstrate the power of our symmetry protected QSRG by applying it to this AKLT phase.

1. Algorithm

The key procedure for the 2D symmetry protected QSRG is schematically the same as the one discussed in IIB for non-SPT, and is recapitulated in Fig. 4 and Fig. 5. As for the 1D case, it contains two steps: disentangling and coarse-graining. Again, the disentangling preserves the on-site symmetries as it acts on the symmetric double tensor. Instead, we should be careful in the process of coarse-graining when splitting the tensor \tilde{T} in Fig. 4 before re-merging. The symmetry properties of the SPT state will manifest in the degeneracy pattern of the singular value spectrum when splitting the tensor \tilde{T} . We may need to enlarge the Hilbert space for the physical legs of the tensor \tilde{T} before splitting, and then split it according to the measured quantum number of the physical legs. After that, as shown in Fig. 5 we merge the three new tensors around a vertex with their physical legs in the same cohomology class as the original one. This completes one round of the symmetry protected QSRG.

Again, for $SO(3)$ on-site symmetry the integer spins and half-integer spins belong to different cohomology classes for classifying SPT phases. Therefore, we should assure that the physical legs of all the tensors in the process of QSRG are in the same class of the spin representation to keep the SPT. For 1D SPT states with $SO(3)$ symmetry, physical legs always have to be integer spins. However for 2D SPT states with $SO(3)$ and translation symmetry, physical legs can be either integer spins or half integer spins, depending on the lattice. The key to preserving SPT order in the 2D QSRG scheme is to keep the spin representation class of the physical leg. Besides, the number of degrees of freedom for TPS is much larger than the ones for MPS, we should truncate the minor singular values to make the numerical computation viable. Of course, the truncation should be performed in accordance with the degeneracy patterns of the singular values to ensure the symmetry property of the SPT. Note that we are keeping only block translation symmetry (not the full translation symmetry) in the RG procedure which is sufficient to preserve the SPT order in AKLT states.

2. 2-dimensional AKLT phase as the example

To demonstrate the power of our symmetry protected QSRG, we should consider a 2D model with SPT phase. The simplest one is the 2D AKLT model [17] on the honeycomb lattice, which has $SO(3)$ on-site symmetry. Its ground state is the 2D AKLT state which is a pos-

sible candidate of the SPT phase as expected from its 1D cousin. Moreover, this AKLT state has a simple TPS representation, see [38] for example.

To be more general, we consider the simple variation of the AKLT model with following Hamiltonian

$$H = \sum_{\langle ij \rangle} [J_1 \vec{S}_i \cdot \vec{S}_j + J_2 (\vec{S}_i \cdot \vec{S}_j)^2 + J_3 (\vec{S}_i \cdot \vec{S}_j)^3] \quad (30)$$

This model corresponds to the AKLT one if $J_1 = 1$, $J_2 = 116/243$ and $J_3 = 16/243$. Obviously, this model has $SO(3)$ on-site symmetry.

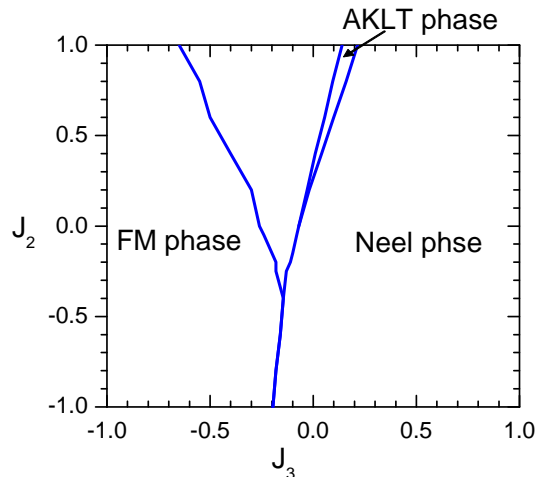


FIG. 10. The phase diagram of the deformed AKLT-like model (30) by tuning J_2 and J_3 with $J_1 = 1$ fixed. The labels Neel, FM and AKLT stand for the Neel, the ferromagnetic and the AKLT phases, respectively.

We solve this model numerically by using the method of simple update [39] for the ground state. We then apply the method of TRG [24] to calculate the order parameters. A typical phase diagram for the (staggered) magnetization is shown in Fig. 11 in which the order parameters goes to zero near $J_3 = 0$. This indicates a possible SPT phase in this regime.

After scanning the parameter space of the Hamiltonian (30) for the order parameters, we finally obtain its total phase diagram as shown in Fig. 10. It indicates there is a phase, we call it the AKLT phase, which does not break the on-site and translational symmetry and could be a possible SPT phase. Now, we will apply our symmetry protected QSRG to give the supporting evidence.

First, if apply the usual QSRG to the ground state of (30), it will flow to the trivial ground state, such as $T_{111}^{111} = 1$. This implies that none of the phases in the phase diagram Fig. 10 has intrinsic topological order.

Then, we apply the symmetry protected QSRG to the 2D AKLT state. The TPS of the AKLT state has the bond dimension $\chi = 2$. After performing the singular value decomposition for the tensor \tilde{T} in Fig. 4, we find that only 9 of the 16 singular values are non-zero. Moreover, these non-zero singular values show the degeneracy

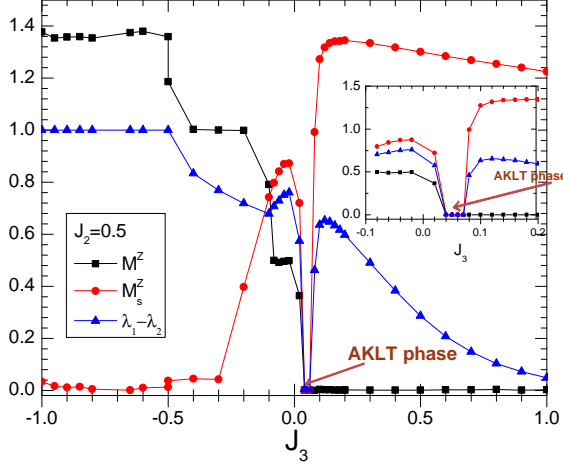


FIG. 11. A typical phase diagram for the magnetization M^z and the stagger magnetization M_s^z by tuning J_2 with $J_1 = 1$ and $J_2 = 0.5$ fixed. We fix the bond dimension $\chi = 4$ and $D_{cut} = 24$ in this numerical calculation. We also plot the difference between the largest two singular values, i.e., $\lambda_1 - \lambda_2$.

pattern as 1-, 3- and 5-fold degeneracies. Similar degeneracy pattern appears also for the other ground states in the AKLT phase. We also check the ground state for the Néel and ferromagnetic phases but find no such degeneracy pattern. This implies that the AKLT phase could be a SPT one protected by the on-site $SO(3)$ symmetry and the translational invariance.

Since the original physical leg is in the half-integer representation, i.e., spin $3/2$, so we should require the physical legs of the tensors in the intermediate steps to be in the half-integer representation to ensure the SPT. The simplest way is to interpret the physical leg of \tilde{T} as comprised of four spin $1/2$ “partons”. Thus, we can understand the degeneracy pattern of the singular values as follows: $2 \otimes 2 \otimes 2 \otimes 2 = 1 \oplus 1 \oplus 3 \oplus 3 \oplus 3 \oplus 5$. Accordingly, we should enlarge the Hilbert space of the physical leg of the tensor \tilde{T} and split it by the rule of the measured quantum number in such a decomposition, e.g., fill empty elements for two of the three 3-representations and one of the two 1-representations.

By this way of performing symmetry protected QSRG on the AKLT state, we finally arrive the following fixed-point double tensor:

$$\begin{aligned}
 T_{111}^{111} &= 0.05; \\
 T_{112}^{112} &= 0.044; & T_{121}^{121} &= 0.044; & T_{211}^{211} &= 0.044; \\
 T_{221}^{221} &= 0.036; & T_{212}^{212} &= 0.036; & T_{122}^{122} &= 0.036; \\
 T_{222}^{222} &= 0.05.
 \end{aligned} \tag{31}$$

We show that this is also the fixed-point double tensor of the 2D dimer state represented by the TPS with the tensor $T_{ijk}^{ijk} = 1$ for $i, j, k = 1, 2$. This phase is the valence bond solid with each pair of “patrons” on the neighboring sites forming singlet state. In the language of TPS,

the projection operator is the identity. We also apply the symmetry protected QSRG to the other numerical ground states in the AKLT phases, they all flow to the same fixed-point state given by (31). This then demonstrate the power of our symmetry protected QSRG and also justify the SPT of the AKLT phase.

IV. CONCLUSION

After so many years’s effort in developing the theoretical perspective of topological order, it is time to explore more the possibilities of realizing either intrinsic or symmetry protected topological order in real materials. To motivate the experimental search, it is better for theorists to find out the possible realistic models which could be fabricated in the real world. As most of the exactly solvable higher dimensional models with (symmetry protected) topologically ordered ground states involve non-realistic interactions, it usually needs numerical computations to find out the possible topologically ordered phases for the more realistic models.

In this paper we have aimed at such a goal in devising a numerical algorithm based on the matrix and tensor product state representation of the ground states. Our new algorithm of the quantum state renormalization can flow a original ground state wave function to its fixed-point state in the same class of the SPT. The fixed-point state is usually simple and universal due to the removal of irrelevant short range entanglements so that it can be used to classify the SPT. This algorithm is the modified version of the original quantum state renormalization [30, 35] to adopt the symmetry constraints in protecting the SPTs. A key observation in our algorithm is to add or remove only the symmetry allowed degrees of freedom when coarse graining the lattice.

We have considered the 1D and 2D AKLT phases as the examples in testing our quantum state renormalization algorithm. These models have on-site $SO(3)$ symmetry so that only integer spins degrees of freedom can be added or removed when coarse graining. Our numerical implantation of the new algorithm on these states yield satisfying results by finding that they all flow the same fixed-point states as the dimer states do. This confirmed that the AKLT and the dimer states are in the same SPT class for the 1D and 2D cases.

Despite of the success of our algorithm, we find that the detailed procedure of the symmetry protected quantum state renormalization algorithm is not unique, and the subtle difference in the procedure will lead to different forms of the fixed-point state. Though this is expected as the expression of the SRE will depend on the choice of the basis and performed local unitary transformations. It is then desired to see if there are some criterions to fix such ambiguity.

Finally, it is interesting to apply our algorithm to more general realistic models in identifying the new SPT phases. Also, it is worthy of devising a new quantum

state renormalization algorithm for the phases with both the intrinsic and symmetry protected topological orders.

ACKNOWLEDGMENTS

We would like to acknowledge discussion with Xiao-Gang Wen and Frank Pollmann. XC is supported by the Miller Institute for Basic Research in Science at UC Berkeley. FLL is supported by Taiwan's NSC grants (grant NO. 100-2811-M-003-011 and 100-2918-I-003-008) and he also thanks the support of NCTS.

Appendix A: Projective Representation

Matrices $u(g)$ form a projective representation of symmetry group G if

$$u(g_1)u(g_2) = \omega(g_1, g_2)u(g_1g_2), \quad g_1, g_2 \in G. \quad (A1)$$

Here $\omega(g_1, g_2) \in U(1)$ and $\omega(g_1, g_2) \neq 0$, which is called the factor system of the projective representation. The factor system satisfies

$$\omega(g_2, g_3)\omega(g_1, g_2g_3) = \omega(g_1, g_2)\omega(g_1g_2, g_3), \quad (A2)$$

for all $g_1, g_2, g_3 \in G$. If $\omega(g_1, g_2) = 1$, this reduces to the usual linear representation of G .

A different choice of pre-factor for the representation matrices $u'(g) = \beta(g)u(g)$ will lead to a different factor system $\omega'(g_1, g_2)$:

$$\omega'(g_1, g_2) = \frac{\beta(g_1g_2)}{\beta(g_1)\beta(g_2)}\omega(g_1, g_2). \quad (A3)$$

We regard $u'(g)$ and $u(g)$ that differ only by a pre-factor as equivalent projective representations and the corresponding factor systems $\omega'(g_1, g_2)$ and $\omega(g_1, g_2)$ as belonging to the same class ω .

Suppose that we have one projective representation $u_1(g)$ with factor system $\omega_1(g_1, g_2)$ of class ω_1 and another $u_2(g)$ with factor system $\omega_2(g_1, g_2)$ of class ω_2 , obviously $u_1(g) \otimes u_2(g)$ is a projective presentation with factor group $\omega_1(g_1, g_2)\omega_2(g_1, g_2)$. The corresponding class ω can be written as a sum $\omega_1 + \omega_2$. Under such an addition rule, the equivalence classes of factor systems form an Abelian group, which is called the second cohomology group of G and denoted as $\mathcal{H}^2[G, U(1)]$. The identity element $1 \in \mathcal{H}^2[G, U(1)]$ is the class that corresponds to the linear representation of the group.

Appendix B: Numerical results for solving 2-dimensional AKLT-like model

We adopt the method of simple update [39] to solve the ground state of (30) numerically. Then, we apply the method of TRG [24] to evaluate the relevant order

parameters and delineate the phase diagrams as shown in Fig. 11 and 13. The total phase diagram of this model as shown in Fig. 10.

We assume the translational invariance for the TPS ansatz for the ground state of (30). Using the simple update method we can solve the TPS numerically. One should caution that the unit cell used in the simple update is a honeycomb, which is different from the acyclic tree of coordination number equal to 3. So, when performing each step of the simple update, we need to update the six kinds of tensors and nine bonds as shown in Fig. 12.

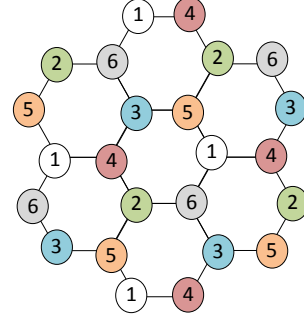


FIG. 12. Diagrammatic representation of the TPS on the honeycomb lattice. The tensors $T^{(i)}$, with $i = 1, 2, \dots, 6$ on the site labeled by i has three bond indices and one physical index.

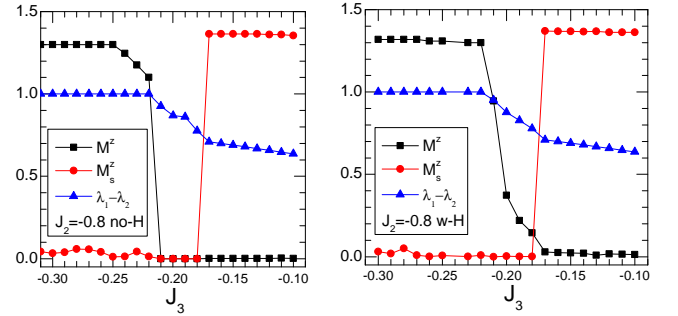


FIG. 13. A typical phase diagram for the magnetization M^z and the stagger magnetization M_s^z by tuning J_3 with $J_1 = 1$ and $J_2 = -0.8$ fixed. We fix the bond dimension $\chi = 4$ and $D_{cut} = 24$ in this numerical calculation. The left one is without annealing but the right one is with annealing by tuning a small magnetic field in the z-direction when evaluating the ground state. This annealing kill the sudden jump of M^z . We also calculate the energy per site for $J_3 = -0.2$. The energies with and without the annealing are -7.303 and -7.150 , respectively.

Based on the numerical solution from simple update we can further use TRG method to evaluate the expectation value of the magnetization denoted by M^z and the staggered magnetization M_s^z . They are the order

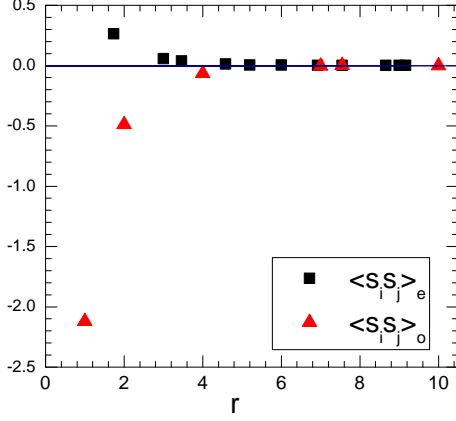


FIG. 14. The spin-spin correlation function as a function of $r = |i-j|$. In this numerical calculation, $\chi = 4$ and $D_{cut} = 24$ are used.

parameters for the ferromagnetic and the Néel phases, respectively. In our numerical calculation, we consider the bond dimension up to $\chi = 5$ and keep $D_{cut} \geq \chi^2$ to ensure the accuracy of the TRG calculation. A typical numerical result for M^z and M_s^z are shown in Fig. 11 with $J_1 = 1$ and $J_2 = 0.5$, which shows a quantum phase transition around $J_3 = 0$ from the Néel phase to the AKLT phase as we decrease J_3 . Note that the difference between largest two singular values also indicates the quantum phase transition. If we further decrease J_3 , we will reach the ferromagnetic phase. We also plot another numerical results with $J_2 = -0.8$ in Fig. 13. It shows that the Néel order will suddenly drop to zero and remain zero after that. On the other hand, the M^z is zero but suddenly start to grow. However, if anneal the result by tuning small magnetic field, then it shows that M^z grows gradually. This indicates there are only the ferromagnetic and the Néel phases in this regime.

We also calculate the spin-spin correlation function at the AKLT point in the Fig 14. It shows the exponentially-decay behavior as expected for a gapped system like the AKLT model.

-
- [1] X. Chen, Z.-C. Gu, Z.-X. Liu and X.-G. Wen, Science **338**, 1604 (2012); arXiv:1106.4772v6.
 - [2] M. Z. Hasan and C. L. Kane, Rev. Mod. Phys. **82**, 3045 (2011).
 - [3] X.-L. Qi and S.-C. Zhang, Rev. Mod. Phys. **83**, 1057 (2011).
 - [4] M. Z. Hasan and J. E. Moore, Annu. Rev. Condens. Matter Phys. **2**, 55 (2011).
 - [5] A. P. Schnyder, S. Ryu, A. Furusaki, and A. W. W. Ludwig, Phys. Rev. B **78**, 195125 (2008).
 - [6] A. Kitaev, AIP Conf. Proc. **1134**, 22 (2009).
 - [7] X.-G. Wen, Phys. Rev. B **85**, 085103 (2012).
 - [8] F. Pollmann, A. M. Turner, E. Berg, M. Oshikawa, Phys. Rev. B **81**, 064439 (2010).
 - [9] X. Chen, Z.-C. Gu, and X.-G. Wen, Phys. Rev. B **83**, 035107 (2010).
 - [10] X. Chen, Z.-C. Gu, and X.-G. Wen, Phys. Rev. B **84**, 235128 (2011).
 - [11] N. Schuch, D. Perez-Garcia, and I. Cirac, Phys. Rev. B **84**, 165139 (2011).
 - [12] A. M. Turner, F. Pollmann, and E. Berg, Phys. Rev. B **83**, 075102 (2011).
 - [13] L. Fidkowski and A. Kitaev, Phys. Rev. B **83**, 075103 (2011).
 - [14] F. Pollmann, E. Berg, A. M. Turner, and M. Oshikawa, Phys. Rev. B **85**, 075125 (2012).
 - [15] F. Haldane, Physics Letters A **93**, 464 (1983).
 - [16] I. Affleck, T. Kennedy, E. H. Lieb, and H. Tasaki, Phys. Rev. Lett. **59**, 799 (1987).
 - [17] I. Affleck, T. Kennedy, E. H. Lieb, and H. Tasaki, Comm. Math. Phys. **115**, 477 (1988).
 - [18] Zheng-Cheng Gu and Xiao-Gang Wen, arXiv:1201.2648v2 [cond-mat.str-el] (2012).
 - [19] X. Chen, Z.-X. Liu, and X.-G. Wen, Phys. Rev. B **84**, 235141 (2011).
 - [20] M. Levin and Z.-C. Gu, Phys. Rev. B **86**, 115109 (2012).
 - [21] F. Verstraete, J.I. Cirac, V. Murg, Adv. Phys. **57**, 143 (2008).
 - [22] J. I. Cirac and F. Verstraete, J. Phys. A **42**, 504004 (2009).
 - [23] G. Vidal, arXiv:0912.1651 [cond-mat.str-el] (2009).
 - [24] M. Levin and C. P. Nave, Phys. Rev. Lett. **99**, 120601 (2007).
 - [25] Z. C. Gu, M. Levin and X. G. Wen, Phys. Rev. B **78**, 205116(2008).
 - [26] F. D. M. Haldane and E. H. Rezayi, Phys. Rev. B **31**, 2529 (1985).
 - [27] X.-G. Wen and Q. Niu, Phys. Rev. B **41**, 9377 (1990).
 - [28] M. Levin and X.-G. Wen, Phys. Rev. Lett. **96**, 110405 (2006).
 - [29] A. Kitaev and J. Preskill, Phys. Rev. Lett. **96**, 110404 (2006).
 - [30] X. Chen, Z.-C. Gu, and X.-G. Wen, Phys. Rev. B **82**, 155138 (2010).
 - [31] C.-Y. Huang and F.-L. Lin, Phys. Rev. B **84**, 125110(2011).
 - [32] K. Hida, Phys. Rev. B **45**, 2207 (1992).
 - [33] M. Kohmoto, and H. Tasaki, Phys. Rev. B **46**, 3486 (1992).
 - [34] S. R. White, Phys. Rev. Lett. **69**, 2863 (1992).
 - [35] F. Verstraete, J. I. Cirac, J. I. Latorre, E. Rico, and M. M. Wolf, Phys. Rev. Lett. **94**, 140601 (2005).
 - [36] A. M. Essin and M. Hermele, arXiv:1212.0953
 - [37] G. Vidal, Phys. Rev. Lett. **99**, 220405 (2007). G. Evenbly and G. Vidal, Phys. Rev. B **79**, 144108 (2009).
 - [38] T.-C. Wei, I. Affleck and R. Raussendorf, Phys. Rev. Lett. **106**, 070501 (2011).
 - [39] G. Vidal, Phys. Rev. Lett. **98**, 070201(2007); R. Orös and G. Vidal, Phys. Rev. B **78**, 155117 (2008).
 - [40] E. L. Lieb, T. Schultz, and D. Mattis, Ann. Phys. **16**,

- 407 (1961).
- [41] M. Nielsen and I. Chuang, *Quantum computation and quantum information* (Cambridge University Press, Cambridge, 2000).
- [42] D. Pérez-García, F. Verstraete, M. Wolf, and J. I. Cirac, Quantum Inf. Comput. **7**, 401 (2007)
- [43] Z.-C. Gu, and X.-G. Wen, Phys. Rev. B. **80**, 155131 (2009).